J. Fluid Mech. (2018), *vol.* 852, *pp.* 663–677.
doi:10.1017/jfm.2018.574

Floquet stability analysis of capsules in viscous shear flow

Spencer H. Bryngelson[1] **and Jonathan B. Freund**[1,2,†]

[1]Department of Mechanical Science and Engineering, University of Illinois at Urbana–Champaign, Urbana, IL 61801, USA

[2]Department of Aerospace Engineering, University of Illinois at Urbana–Champaign, Urbana, IL 61801, USA

(Received 11 April 2018; revised 11 April 2018; accepted 13 July 2018)

Observations in experiments and simulations show that the kinematic behaviour of an elastic capsule, suspended and rotating in shear flow, depends upon the flow strength, the capsule membrane material properties and its at-rest shape. We develop a linear stability description of the periodically rotating base state of this coupled system, as represented by a boundary integral flow formulation with spherical harmonic basis functions describing the elastic capsule geometry. This yields Floquet multipliers that classify the stability of the capsule motion for elastic capillary numbers Ca ranging from $Ca = 0.01$ to 5. Viscous dissipation rapidly damps most perturbations. However, for all cases, a single component grows or decays slowly, depending upon Ca, over many periods of the rotation. The transitions in this stability behaviour correspond to the different classes of rotating motion observed in previous studies.

Key words: biological fluid dynamics, capsule/cell dynamics

1. Introduction

Thin elastic membranes enclosing liquids, which have come to be called capsules, are central to many applications. They are manufactured for purposes such as inkjet printing (Leelajariyakul, Noguchi & Kiatkamjornwong 2008), use in cosmetics (Miyazawa *et al.* 2000; Martins *et al.* 2014), releasing aromas and flavours (Gibbs *et al.* 1999; Pop 2011) and absorbing CO_2 in gas plumes (Vericella *et al.* 2015). Similarly, they are attractive for biomedical applications, including drug delivery (Lim 1984; Dey, Majumdar & Rao 2008; Paret *et al.* 2015), contrast-enhanced ultrasound imaging (Furlow 2009) and the development of artificial blood and organs (Kuhtreiber, Lanza & Chick 1998; Chang 2010). The collective flow of such suspensions depends upon the dynamics of the capsules, which has motivated extensive studies (Barthès-Biesel 2016). The stability of the capsule motion when subject to shear flow is expected to be important for their behaviour, either in isolation or in dense suspensions. If the capsule motion is steady or periodic for particular flow conditions, we anticipate less overall flow resistance than if it is fundamentally unstable. Unsteady capsule motion can also be expected to cause additional stress

† Email address for correspondence: jbfreund@illinois.edu

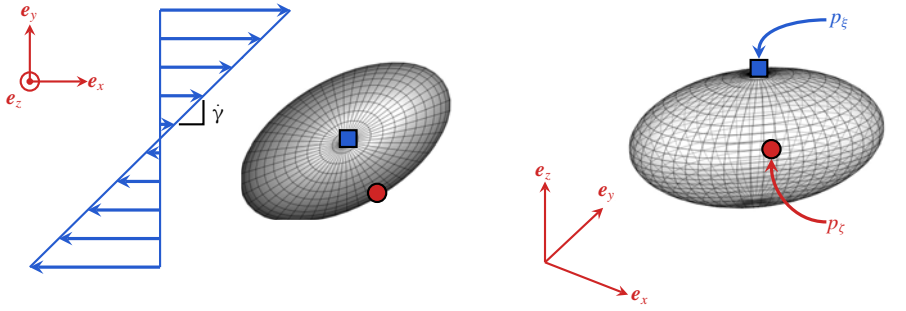

FIGURE 1. (Colour online) The capsule–homogeneous-shear-flow configuration; p_ξ and p_ζ are points used to define deformation and motion in § 2.

on the capsule membranes themselves, which are often fragile (Goosen *et al.* 1985; Gåserød, Sannes & Skjåk-Bræk 1999). Studies of capsule stability have been based on observations, especially in simulation models. We develop a complementary direct stability analysis of the coupled capsule–shear-flow system. Similarly to the primarily empirical studies that guide us, our analysis is based on numerical methods. However, these methods are used here to construct a linearized system for analysis, which is advantageous in that it predicts the linear behaviour of the complete basis of membrane perturbations included in the numerical discretization, not necessarily just those directly observed in flow simulations.

We consider both spherical and ellipsoidal capsules in homogeneous shear flow, as shown schematically in figure 1. This configuration can produce rich and varied capsule kinematics, depending upon the capsule shape and flow strength (Dupont, Salsac & Barthès-Biesel 2013). Simulation-based studies have both considered the viscous Stokes-flow limit (Dupont *et al.* 2013, 2016) and included finite inertia (Cordasco & Bagchi 2013; Wang *et al.* 2013); here, we only consider the viscous limit. For prolate capsules, weak flow and long times, capsules have been observed to reach an apparently steady rolling or tank-treading motion, for which the membrane rotates in the shear plane about a deformed capsule shape (Dupont *et al.* 2013). Such a configuration is visualized in figure 1, with $\boldsymbol{e}_x$–$\boldsymbol{e}_y$ spanning the nominal shear plane. For stronger shear, in addition to rotation, the capsule also precesses around the base-flow vorticity axis ($\boldsymbol{e}_z$), and for still stronger shear, a so-called swinging motion is observed, where a time-periodic deformation cycle appears in addition to the tank-treading motion (Dupont *et al.* 2013; Wang *et al.* 2013). Oblate capsules have been observed to undergo similar motion at long times (Cordasco & Bagchi 2013; Wang *et al.* 2013; Dupont *et al.* 2016). For weak flows, oblate capsules take on a swinging motion, and can wobble with increasing shear rate. In this case, the capsule orientation oscillates about an axis not aligned with the shear-flow vorticity. For sufficiently strong shear rates, the capsule rolls, its deformed membrane rotating about the $\boldsymbol{e}_z$ axis (Dupont *et al.* 2016).

Simulations suggest that the long-time capsule orientation and cyclic motion are independent of the initial capsule orientation, as quantified by the angle of the longest principal axes of a fitted ellipsoid with respect to the shear plane (Dupont *et al.* 2013, 2016). However, there is some ambiguity in reported results (Cordasco & Bagchi 2013), which has been hypothesized to result from insufficient observation times (Dupont *et al.* 2016). It is a challenge with finite-time simulations to determine

unambiguously that longer times do not yield qualitatively different conclusions. Such observations also do not directly classify the stability, and risk missing kinematic behaviour that might be sensitive to initial perturbations. Particular deformations are known to be unstable in other flows, such as a slender capsule subjected to strong extensional flow (Zhao & Shaqfeh 2013) and capsule trains flowing within channels (Bryngelson & Freund 2016) and tubes (Bryngelson & Freund 2018). Our goal is to classify the stability of capsules in shear flow based on analysis of the corresponding linear system. We develop a linear stability analysis that includes a complete basis (for the selected spatial resolution) of capsule membrane perturbations, as represented with spherical harmonic functions. This is used to determine the rate at which perturbations grow or decay.

We consider perturbations to the fixed-point configurations deduced in previous simulation studies (Dupont *et al.* 2016) and analyse the stability of the periodic rotation with Floquet methods. Similar methods have been used to classify the stability of flow in periodically forced lid-driven cavities (Cazemier, Verstappen & Veldman 1998; Blackburn & Lopez 2003), periodic vortex streets shed by rings (Sheard, Thompson & Hourigan 2003, 2004) and square and circular cylinders (Barkley & Henderson 1996; Gioria *et al.* 2009; Sheard, Fitzgerald & Ryan 2009), pulsatile channel (Von Kerczek 1982; Pier & Schmid 2017) and pipe flows (Blennerhassett & Bassom 2007; Thomas, Bassom & Blennerhassett 2012), and Stokes layers adjacent to oscillating boundaries (Blennerhassett & Bassom 2002; Davies *et al.* 2015; Thomas *et al.* 2015). These studies generally rely to some degree upon numerical methods, as does ours. Few Floquet studies include fluid–structure interaction; the present analysis is perhaps most closely related to the Floquet analysis of axisymmetric rigid particles in shear flow with weak inertia (Einarsson, Angilella & Mehlig 2014), although in that case the rigid-particle dynamics allows for a tractable analytic linearization of the governing equations about the periodic particle motion. The deformable membrane introduced here presents additional complexity that seems to preclude direct extension of that formulation.

The details of the specific configurations we consider are introduced in § 2. The numerical methods used for constructing the periodic base flow, the stability analysis and the corresponding direct numerical simulations (DNS) are summarized in § 3. We verify that our simulations reproduce particular results of previous studies in § 4; these also provide the time-periodic base flows for our subsequent Floquet analysis. The stability analysis is developed in § 5, with results presented in § 6 for a range of flow strengths.

2. Capsule–flow system

The initial capsule shape $\boldsymbol{x} = \{x, y, z\}$ in figure 1 is a spheroid with

$$\frac{x^2 + y^2}{b^2} + \frac{z^2}{a^2} = 1, \tag{2.1}$$

where a/b is the aspect ratio and $r_o = (b^2 a)^{1/3}$ is the radius of a sphere of the same volume. The capsule perturbs a homogeneous shear flow,

$$\boldsymbol{u}^\infty(\boldsymbol{x}) = \dot{\gamma} y \boldsymbol{e}_x, \tag{2.2}$$

where $\dot{\gamma}$ is the shear rate. Following Dupont *et al.* (2016), we define $\zeta(t)$ as the instantaneous angle between the $\boldsymbol{e}_z$ axis and the shortest capsule principal axis.

Similarly, $\xi(t)$ is the angle between the $\boldsymbol{e}_z$ axis and a segment extending from the capsule centre to the point that was initially on the shortest principal axis at time $t=0$. The corresponding points on the capsule are p_ζ and p_ξ, as labelled in figure 1. Both the interior and the exterior fluid are Newtonian and incompressible with the same viscosity μ.

The capsule membrane elastic resistance is described using the Skalak constitutive model (Skalak *et al.* 1973) with strain energy

$$W = \frac{E_s}{8}(I_1^2 + 2I_1 - 2I_2) + \frac{E_d}{8}I_2^2, \tag{2.3}$$

where E_s is the shear modulus, $E_d = CE_s$ is the dilatation modulus (where C sets its relative strength) and $I_{1,2}$ are the usual strain invariants. Bending is resisted through a linear isotropic model (Zhao *et al.* 2010) with bending moment

$$\boldsymbol{M} = -E_b(\boldsymbol{\kappa} - \boldsymbol{\kappa}^R), \tag{2.4}$$

where E_b is the bending modulus, $\boldsymbol{\kappa}$ is the second fundamental form of the surface (the covariant component of the Riemann curvature tensor) and $\boldsymbol{\kappa}^R$ is the corresponding second fundamental form of the reference shape (2.1). We take $E_b = 5 \times 10^{-3} E_s r_o^2$, which reflects values of typical capsules (Walter, Rehage & Leonhard 2001; Guckenberger & Gekle 2017), except for select cases in § 4, for which $E_b = 0$ is used to facilitate comparison with other studies. An elastic capillary number $Ca \equiv 2\dot{\gamma}\mu r_o/E_s$ serves as a measure of flow strength, with the factor of 2 included to match previous definitions (Lac *et al.* 2004; Dupont *et al.* 2016).

3. Numerical methods

The capsule membrane shape is represented by a sum of spherical harmonics as

$$\boldsymbol{x}(\theta, \phi) = \sum_{n=0}^{N-1} \sum_{m=0}^{n} \widetilde{P}_n^m(\sin\theta)(\boldsymbol{a}_{nm}\cos m\phi + \boldsymbol{b}_{nm}\sin m\phi), \tag{3.1}$$

where $\boldsymbol{x}$ defines the capsule surface, $\widetilde{P}_n^m$ are normalized Legendre polynomials, and $\boldsymbol{a}_{nm}$ and $\boldsymbol{b}_{nm}$ are coefficients The relatively small number of modes required to accurately describe the capsule shape and the mutual orthogonality of the spherical harmonic basis functions are important for our stability formulation and analysis.

Here, we use $N = 8$, although three times this amount is carried for dealiasing nonlinear evaluations in the simulations we present (Zhao *et al.* 2010); we verify that the instability amplification rates of § 6 vary by less than 2 % for $N = 10$. The coefficients are represented compactly as $\boldsymbol{s} = \{a_{nm}^{(i)}, b_{nm}^{(i)}\}$, where $i = 1, 2, 3$ is the coordinate direction index, $n \geqslant m$ per (3.1), and irrelevant b_{n0} are omitted from $\boldsymbol{s}$ for all n; together, these give $\boldsymbol{s}$ a total of $3N^2$ components. The membrane collocation points $\boldsymbol{x} = \{x^{(i)}(\theta_k, \phi_l)\}$ for coordinate direction $i = 1, 2, 3$ are computed by (3.1) with $\theta_k \in (0, \pi)$ for $k = 1, \ldots, N$ colatitudinal Gauss points and $\phi_l \in [0, 2\pi)$ for $l = 1, \ldots, 2N$ uniformly spaced longitudinal points (Adams & Swarztrauber 1997). The forward and reverse discrete spherical harmonic transforms are compactly expressible as

$$\boldsymbol{x} = \boldsymbol{B}\boldsymbol{s} \quad \text{and} \quad \boldsymbol{s} = \widetilde{\boldsymbol{B}}\boldsymbol{x}. \tag{3.2a,b}$$

The Reynolds numbers of capsule flows are often much less than unity, so inertia is neglected and the velocity of the capsule surface, $\boldsymbol{u}(\boldsymbol{x})$, is represented with standard

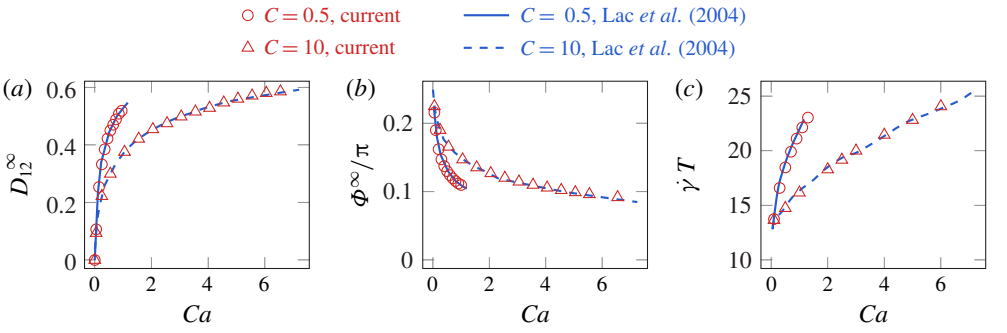

FIGURE 2. (Colour online) Comparison with Lac *et al.* (2004) for $a/b = 1$ and Ca and C as indicated: (*a*) Taylor parameter, (*b*) inclination angle and (*c*) rotation period (see text).

boundary integrals (Rallison & Acrivos 1978; Kim & Karrila 1991; Pozrikidis 1992), which are discretized and evaluated using a quadrature scheme for the collocation points $\boldsymbol{x}$ (Freund & Zhao 2010). The free-space Green's function of the Stokes equation is evaluated directly for all interactions. With the velocity computed from the boundary integral evaluation, the capsule surface moves simply as

$$\frac{\mathrm{d}\boldsymbol{x}}{\mathrm{d}t} = \boldsymbol{u}(\boldsymbol{x}), \tag{3.3}$$

which in our simulations is integrated in time with the forward Euler method $\boldsymbol{x}^{j+1} = \boldsymbol{x}^{j} + \Delta t\, \boldsymbol{u}(\boldsymbol{x}^{j})$, where $\Delta t = 10^{-3}T$ is the time step and T is the period of the capsule motion.

4. Cycles of capsule motion

We construct periodic base states of the capsule motion for cases with capillary number Ca, dilatational resistance factor C and aspect ratio a/b selected to match commonly studied configurations, which also serves to facilitate verification of our numerical method and stability formulation. First, we take a spherical capsule ($a/b = 1$) and compare with Lac *et al.* (2004). The capsule motion and deformation are quantified by the Taylor parameter,

$$D_{ij}(t) \equiv \frac{|L_i(t) - L_j(t)|}{L_i(t) + L_j(t)}, \tag{4.1}$$

where the L_i are the principal axes of the linear least-squares fitted ellipsoid of the capsule (with eigenvalues decreasing from $i = 1$ to $i = 3$), the inclination angle Φ of L_1 with respect to the flow direction $\boldsymbol{e}_x$, and the period of the capsule rotation T. The period is calculated such that $\|\boldsymbol{s}[t] - \boldsymbol{s}[t+T]\| < 10^{-4}$, where $\|\cdot\|$ indicates an L^2 norm. Long-time values are denoted by D_{ij}^{∞} and Φ^{∞}, and these preparatory simulations are run until D_{12}^{∞} and Φ vary by less than 0.1 % over a T period.

Figure 2 shows that D_{12}^{∞}, Φ^{∞} and T match closely with those of Lac *et al.* (2004). For this comparison, we do not include membrane bending resistance ($E_b = 0$), consistent with their simulations. As a result, the capsule membrane buckles (Walter *et al.* 2001; Lac *et al.* 2004; Barthès-Biesel 2009; Foessel *et al.* 2011) and forms features at the scale of the numerical discretization. As such, it is potentially sensitive

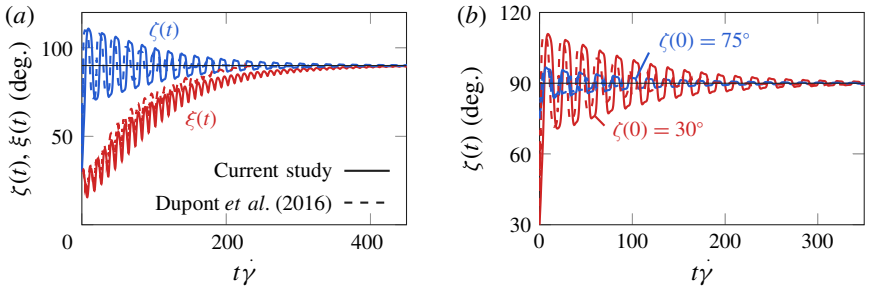

FIGURE 3. (Colour online) Cases with $a/b = 0.5$, $C = 1$, $E_b = 0$ and $Ca = 0.3$: (*a*) $\xi(0) = \zeta(0) = 30°$ and (*b*) $\zeta(0) = 30°$ and $75°$.

to the mesh (Barthès-Biesel 2009; Dupont *et al.* 2016). However, such sensitivity is not seen in figure 2 for a spherical capsule, where the results of our dealiased spectral method match those of the finite-element description (Lac *et al.* 2004).

Oblate capsules with $a/b = 0.5$ will also be considered as reference configurations for the subsequent stability analysis, and they are compared with the results of Dupont *et al.* (2016) in figure 3. The evolving principal axis angles $\xi(t)$ and $\zeta(t)$ are qualitatively similar to their reported results. However, for $t\dot{\gamma} \gtrsim 400$, our results approach the same $\zeta = \xi = 90°$ values. We hypothesize that the small differences for $t\dot{\gamma} \lesssim 300$ are due to differences in the numerical methods, as the capsules do not resist bending and buckle with features with wavelengths comparable to the spatial discretization. As such, the numerical smoothing (or artificial membrane stiffness) at the length scales of the discretization, characteristic of finite-element methods, could explain the differences. The spherical harmonic basis functions and dealiasing procedure used here minimize numerical smoothing, although our method still truncates the spherical harmonic series at degree N. We confirm that the presented $\zeta(t)$ and $\xi(t)$ for $t\dot{\gamma} \lesssim 300$ vary by less than 3 % on increasing to $N = 10$, and note that only the long-time behaviour is important for the primary objectives of our analysis. We also include finite E_b in all subsequent calculations.

With agreement established with previous simulations, we focus on cases with $a/b = 0.5$, $C = 1$, and Ca ranging from 0.01 to 5, commensurate with previous empirical studies of capsule stability (Dupont *et al.* 2016). Our small $E_b = 5 \times 10^{-3} E_s r_o^2$ is both realistic and suppresses short-wavelength buckling, consistent with the absence of buckling reported in experimental observations (Barthès-Biesel 2009). It also provides a physical regularization that removes mesh dependence from the linear stability analysis (§ 5). We analyse capsules initiated with both $\zeta(0) = \xi(0) = 0°$ and $\zeta(0) = \xi(0) = 90°$, which are anticipated fixed points of the capsule motion (Barthès-Biesel 2016).

The base capsule motion is visualized for select cases in figure 4 and classified for the range of Ca we consider in figure 5. The capsules tumble, swing, tank-tread or roll, as defined by Dupont *et al.* (2016). Capsules initiated with $\zeta(0) = \xi(0) = 0°$ roll for all values of Ca considered. In contrast, cases with $\zeta(0) = \xi(0) = 90°$ have qualitatively different motion depending upon Ca: for $Ca \lesssim 0.2$, the capsule tumbles; for $0.2 \lesssim Ca \lesssim 0.9$, it swings; for $Ca \gtrsim 0.9$, it tank-treads. For sufficiently large Ca, the tank-treading behaviour is visually indistinguishable from a rolling motion, although it can be uniquely identified by tracking p_ξ. These base flows are all time periodic per our specification, and as such are analysed with Floquet methods.

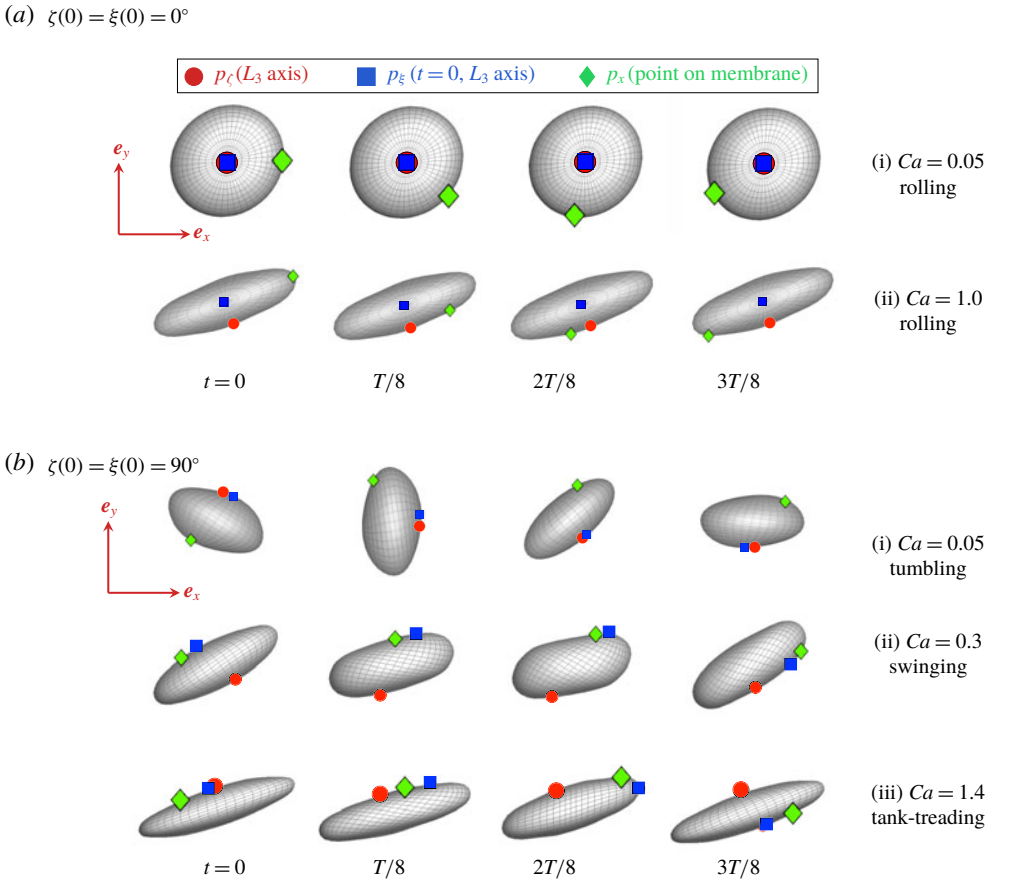

FIGURE 4. (Colour online) Visualizations of capsules over one half-period $T/2$ for Ca as labelled and (*a*) $\zeta(0) = \xi(0) = 0°$ and (*b*) $\zeta(0) = \xi(0) = 90°$. The p_x point is fixed on the membrane surface at $z = 0$.

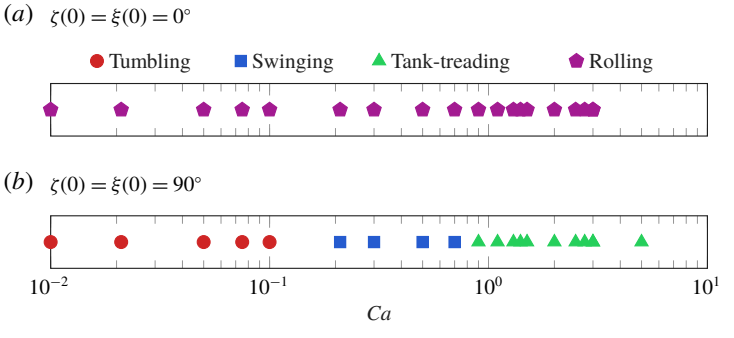

FIGURE 5. (Colour online) Base-flow capsule behaviour (see text) for $a/b = 0.5$, $C = 1$ and initial orientations as labelled.

5. Floquet analysis formulation

The formulation is based upon that developed to analyse steadily flowing red blood cell trains (Bryngelson & Freund 2016, 2018), although here it is extended to include the time-periodic rotation of the capsule. In overview, the linearization proceeds by introducing $\boldsymbol{\delta}[t]$ as a small perturbation to $\boldsymbol{s}[t]$. Expansion of (3.3) and linearization yields

$$\boldsymbol{A}[t]\boldsymbol{\delta}[t] = \widetilde{\boldsymbol{B}}\{\boldsymbol{u}(\boldsymbol{B}\{\boldsymbol{s}[t] + \boldsymbol{\delta}[t]\}) - \boldsymbol{u}(\boldsymbol{B}\boldsymbol{s}[t])\}. \tag{5.1}$$

A full-rank orthogonal set of perturbations $\boldsymbol{\delta}_i$ are used sequentially to calculate each column i of matrix $\boldsymbol{A}[t]$ at time t. For the results presented, we take $\|\boldsymbol{\delta}[t]\| = \delta = 10^{-3}$, and $\boldsymbol{A}[t]$ is evaluated at $j = 1, \ldots, N_t$ uniformly spaced times $t_j = (j-1)T/(N_t - 1)$ with $N_t = 10^4$. Results are insensitive to these specific choices of numerical parameters. With $\boldsymbol{A}$ so determined, the evolution of any small perturbation to the spherical harmonic coefficients $\boldsymbol{\varepsilon}[t]$ is then governed by

$$\frac{\mathrm{d}\boldsymbol{\varepsilon}[t]}{\mathrm{d}t} = \boldsymbol{A}[t]\boldsymbol{\varepsilon}[t]. \tag{5.2}$$

Since $\boldsymbol{A}[t]$ is periodic, (5.2) is a canonical Floquet system with solution of the form

$$\boldsymbol{\varepsilon}[t] = \boldsymbol{X}[t]\boldsymbol{\varepsilon}_o, \tag{5.3}$$

where $\boldsymbol{X}[t]$ is the fundamental solution matrix. Following usual procedures (e.g. Verhulst 2006), we assume that $\boldsymbol{\varepsilon}[t]$ has the form

$$\boldsymbol{\varepsilon}[t] = \sum_{i=1}^{3N^2} c_i \boldsymbol{p}_i[t] \exp \mu_i t, \tag{5.4}$$

where c_i are constants, μ_i are exponential growth rates and $\boldsymbol{p}_i[t]$ are unknown periodic functions. Periodicity requires

$$\boldsymbol{X}[t+T] = \boldsymbol{X}[t]\boldsymbol{X}^{-1}[0]\boldsymbol{X}[T] = \boldsymbol{X}[t]\boldsymbol{C}, \tag{5.5}$$

where $\boldsymbol{C} = \boldsymbol{X}^{-1}[0]\boldsymbol{X}[T]$ is the monodromy matrix (Liu 2003; Verhulst 2006). Substitution of (5.3) into (5.2) yields a system to be solved for $\boldsymbol{X}[t]$,

$$\frac{\mathrm{d}\boldsymbol{X}[t]}{\mathrm{d}t} = \boldsymbol{A}[t]\boldsymbol{X}[t]. \tag{5.6}$$

A key to Floquet analysis is that the stability properties can be determined independently of the initial condition $\boldsymbol{X}[0]$ (Liu 2003; Verhulst 2006); we follow the usual practice of selecting identity $\boldsymbol{X}[t_1 = 0] = \boldsymbol{I}$, so $\boldsymbol{C} = \boldsymbol{X}[T]$ is the principal fundamental matrix. In our calculations, $\boldsymbol{X}[t_{N_t} = T]$, and thus $\boldsymbol{C}$, is found by integrating (5.6). For this, we use the trapezoidal rule $(2\boldsymbol{I} - \Delta t\boldsymbol{A}[t_{j+1}])\boldsymbol{X}[t_{j+1}] = (2\boldsymbol{I} + \Delta t\boldsymbol{A}[t_j])\boldsymbol{X}[t_j]$, which preserves time reversibility and thus does not introduce numerical dissipation. The eigenvalues $\rho_i = \exp \mu_i T$ of $\boldsymbol{C}$ are the Floquet multipliers, the factors by which $\|\boldsymbol{\varepsilon}[t]\|$ for component i of (5.4) grows or decays over a period. Components with $|\rho_i| > 1$ are unstable.

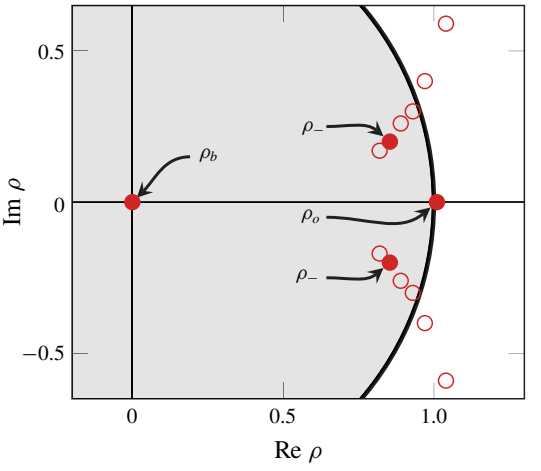

FIGURE 6. (Colour online) The spectrum of $\boldsymbol{C}$ for $a/b = 0.5$, $C = 1$, $Ca = 1.4$ and $\xi(0) = 0°$. The ρ are categorized as neutrally (ρ_o), modestly (ρ_-) or very (ρ_b) stable (see text). Open symbols are ρ_- for Ca between 0.5 and 2.

6. Results

We first consider the $a/b = 0.5$ capsules of § 4, example Floquet multipliers for which are shown in figure 6. There is a complex conjugate pair of modestly stable multipliers $|\rho_-| = 0.84$, which decay over many periods of the rotating capsule motion, and a neutrally stable multiplier $\rho_o = 1$; these have associated eigenvectors $\boldsymbol{v}_-$ and $\boldsymbol{v}_o$ respectively. Neutrally stable multipliers are only determined within the accuracy of our calculations, which for this case is within $\rho_o = 1 \pm 10^{-2}$. This is a result of the approximations introduced by the finite δ used when constructing $\boldsymbol{A}$, the discretization of $\boldsymbol{A}[t]$ in time, and the convergence of the periodic base-flow motion; the coupling between these errors makes quantification of their relative importance challenging, although the details of the coupling are not directly relevant to the conclusions of this paper. For example, if the nominally neutral modes were in fact mildly unstable within this constraint, they would require $t > 700T$ – over 700 periods of rotation – to amplify by a linear mechanism from an initial perturbation amplitude $\hat{\varepsilon} = 10^{-3}$ to unity. Thus, this accuracy is taken to be sufficient to support our conclusions. All other Floquet multipliers of figure 6 are very stable and have $|\rho| \approx 0$, with their associated perturbations vanishing (within the accuracy of our methods) well before a single period T.

Figure 7(*a*) confirms agreement between the linear theory and DNS for the $\boldsymbol{v}_o$ and $\boldsymbol{v}_-$ modes, which serves as a verification of our procedures. We also include one of the $|\rho| \approx 0$ modes, labelling it $\boldsymbol{v}_b$, and confirm that it decays so fast that the finite precision of the calculations make it impossible to confirm its specific behaviour at the end of a T period. The ρ_b are thus unimportant for multiperiod behaviour.

The eigenvector $\boldsymbol{v}_-$, visualized in figure 7(*b*ii), is a tilt of the capsule about the $\boldsymbol{e}_y$ axis, and, in contrast, the $\boldsymbol{v}_b$ is a shorter-wavelength deformation of the capsule. We anticipate the rapid decay of $\boldsymbol{v}_b$ to be due to viscously damped elastic recovery. The decay rate of elastic perturbations can be estimated in the absence of shear flow to decay by more than a factor of 100 over time T (Rochal, Lorman & Mennessier 2005; Zhao *et al.* 2010), matching our observations. The eigenvector $\boldsymbol{v}_o$ is simply

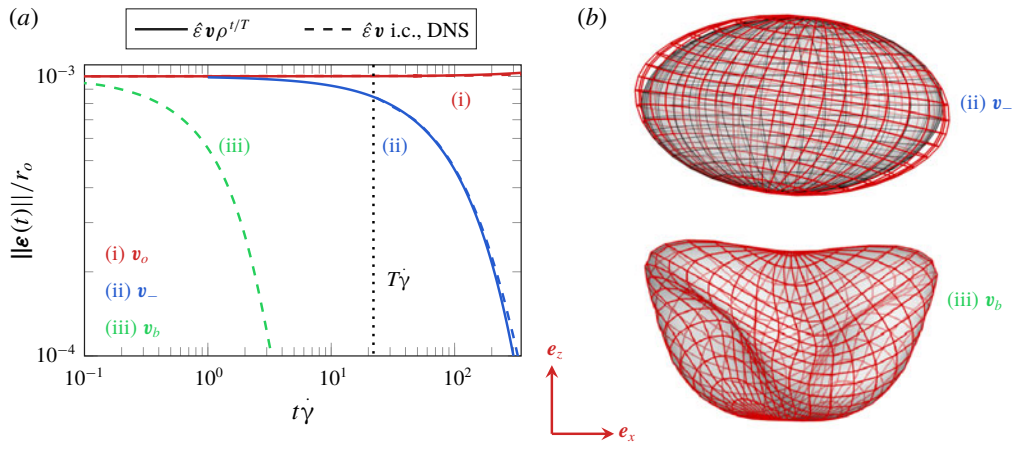

FIGURE 7. (Colour online) (*a*) Linear prediction and DNS for an initial condition (i.c.) associated with the eigenvectors of example Floquet multipliers as labelled for several T periods for $a/b = 0.5$, $C = 1$, $Ca = 1.4$ and $\xi(0) = 0°$. The $t = T$ point is indicated by a dotted line. (*b*) The corresponding eigenvectors (ii) $\boldsymbol{v}_-$ and (iii) $\boldsymbol{v}_b$, magnified as $\boldsymbol{s}[0] + 5\boldsymbol{v}$ for visualization.

an advancement of the capsule surface in the rolling direction, and thus its neutral stability is expected. As such, we focus upon $\boldsymbol{v}_-$.

For the full range of Ca, for both orientations and aspect ratios, each case has one and only one ρ_--like complex conjugate pair of Floquet multipliers; these $|\rho_-|$ are shown in figure 8. A least-squares quadratic fit of the five values closest to $|\rho_-| = 1$ gives a critical value of $Ca_c^{(1)} = 0.82$ for the stable–unstable transition for $a/b = 0.5$, and correspondingly $Ca_c^{(1)} = 0.61$ for $a/b = 0.6$. This is consistent with the trend noted by Dupont *et al.* (2016), who observed stable swinging at larger Ca for smaller a/b. The ρ_- are complex at $|\rho_-| = 1$, as shown in figure 6; this is indicative of a subcritical Neimark–Sacker bifurcation, for which a spiral fixed point changes stability and produces a limit cycle (Sacker 1964). We note that while the bifurcation is clear, the $\boldsymbol{v}_-$ shape and the perturbed velocity field do not qualitatively change near $Ca_c^{(1)}$.

For $\xi(0) = 0°$, the rolling motion is unstable for $Ca < Ca_c^{(1)}$, with $|\rho_-|$ increasing with Ca for $Ca < Ca_c^{(2)}$, where $Ca_c^{(2)} = 0.13$ for $a/b = 0.5$ and $Ca_c^{(2)} = 0.08$ for $a/b = 0.6$. It otherwise decreases with Ca. For $Ca > Ca_c^{(1)}$, $|\rho_-| < 1$ indicates stable rolling. This behaviour reverses for $\xi(0) = 90°$ in figure 8(*b*), where we see that the tumbling and swinging motions of $Ca < Ca_c^{(1)}$ are stable, with $|\rho_-|$ decreasing with Ca in the tumbling regime ($Ca < Ca_c^{(2)}$, where in this case $Ca_c^{(2)} = 0.21$ for $a/b = 0.5$ and $Ca_c^{(2)} = 0.14$ for $a/b = 0.6$). For $Ca > Ca_c^{(1)}$, we have $|\rho_-| > 1$, so tank treading is unstable. For very small $Ca < 0.01$, $|\rho_-| \to 1$ for both the tumbling and rolling motions, even as the period T becomes larger, suggesting that in the $Ca \to 0$ limit, both are neutrally stable. The stability of the tumbling and swinging motions, as well as the large-Ca rolling motion, matches the observed long-time behaviour (Wang *et al.* 2013; Dupont *et al.* 2016), which confirms that nothing was missed by these more empirically grounded studies.

7. Discussion and conclusions

The Floquet analysis was designed to quantify (and clarify) the long-time behaviour of capsules in viscous shear flow, motivated in part by the challenges of performing

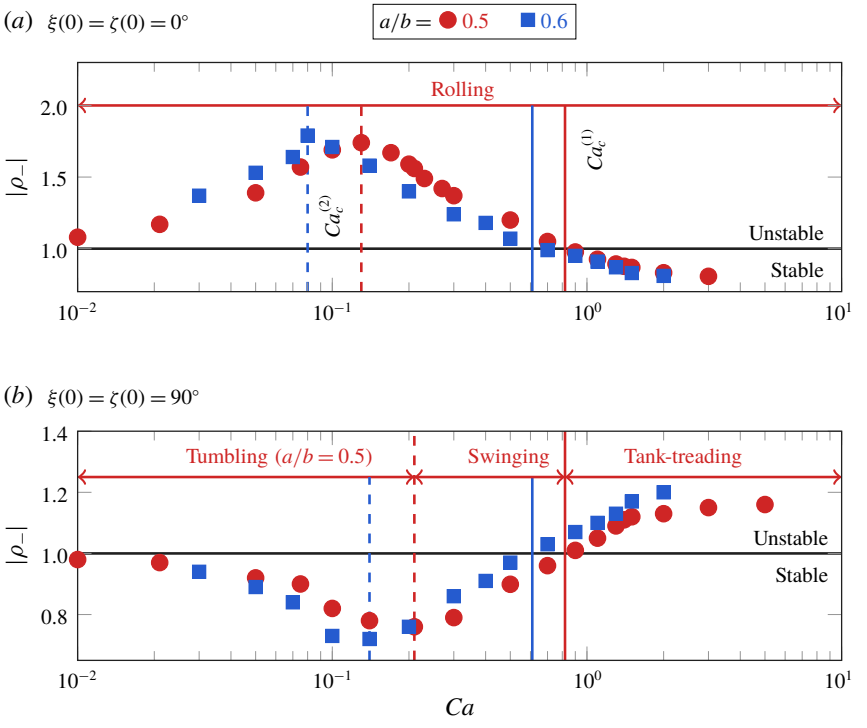

FIGURE 8. (Colour online) Floquet multiplier $|\rho_-|$ for the full range of Ca, $a/b = 0.5$ and 0.6, and (*a*) $\xi(0) = 0°$ and (*b*) $\xi(0) = 90°$. The vertical lines indicate —— $Ca_c^{(1)}$ and – – – $Ca_c^{(2)}$ (see text).

and interpreting corresponding long-time simulations. This has not before been undertaken for this flow. For all cases, most Floquet multipliers are nondescript membrane deformations that rapidly decay with $|\rho| \ll 1$, and thus dissipate within one period of the base capsule motion. This is also consistent with observations of actual capsules, which can rapidly achieve a cyclic behaviour (Walter *et al.* 2001). An expected neutrally stable mode corresponding to a simple rotation of the capsule surface in the flow direction was likewise found. The most interesting mode was the ρ_- complex conjugate pair, which decays or grows over several periods. A single such pair was identified for every set of parameters in the ranges evaluated, although there has not yet been a formal or extensive search for other possible behaviour for other configurations. In all cases, stability was quantified as it depends upon Ca, aspect ratio a/b and the initial capsule orientation $\xi(0)$, with the stable cases matching the long-time behaviour previously observed.

Our stability formulation is perturbation based and includes coupling between a full-rank set of perturbations and the base flow, so its construction is relatively expensive even for simple flows. Data-driven methods, such as those utilizing dynamic mode decompositions (Schmid 2010; Bagheri 2013; Pumhössel, Hehenberger & Zeman 2014) or Koopman operator techniques (Rowley *et al.* 2009; Bagheri 2013), have proved useful if a base flow is unavailable or full construction of the linear stability analysis is prohibitively expensive. These methods determine the most unstable growth rate through a series of temporal realizations of the evolution to disordered flow. Often, only a relatively small number of such realizations is

required, making such analysis computationally efficient. Further, direct computation of perturbations to the flow, or construction of an accurate base flow, is not required. However, such analyses cannot quantify the decay rate for a full-rank set of perturbations to the system, since the dynamics is dominated by the most unstable flow behaviour. Although the information they supply is thus limited, we expect that such methods might be particularly useful for large systems, such as many-capsule flows. Of course, advancement in computational capabilities will also facilitate larger-scale direct analyses and perhaps facilitate the discovery of still richer behaviour.

While the formulation presented here was limited to time-periodic base flows, methods for relaxing this restriction to time-general flows exist, although they are challenging since they do not admit the simplifications of Floquet's theorem. They typically either require analysis of the fundamental matrix operator directly over long times through a singular-value decomposition (Schmid & Kytomaa 1994; Schmid & Henningson 2012) or utilize adjoint operators through an inverse process known as adjoint looping (Juniper 2011). Such analyses are generally more computationally expensive than those for the analogous time-stationary or time-periodic flows, although they are potentially tractable with the methods presented here. Extension of our formulation in this respect would then be appropriate for any non-time-periodic capsule flow, such as that of biconcave capsules in sufficiently strong steady (Skotheim & Secomb 2007) or oscillatory shear flow (Dupire, Abkarian & Viallat 2010), or single vesicles flowing in narrow confines (Aouane *et al.* 2014).

Acknowledgement

This work was supported in part by the National Science Foundation under grant no. CBET 13-36972.

REFERENCES

Adams, J. C. & Swarztrauber, P. N. 1997 SPHEREPACK 2.0: a model development facility. *Tech. Rep.* NCAR/TN-436-STR. NCAR.

Aouane, O., Thiébaud, M., Benyoussef, A., Wagner, C. & Misbah, C. 2014 Vesicle dynamics in a confined Poiseuille flow: from steady state to chaos. *Phys. Rev.* E **90** (3), 033011.

Bagheri, S. 2013 Koopman-mode decomposition of the cylinder wake. *J. Fluid Mech.* **726**, 596–623.

Barkley, D. & Henderson, R. D. 1996 Three-dimensional Floquet stability analysis of the wake of a circular cylinder. *J. Fluid Mech.* **322**, 215–241.

Barthès-Biesel, D. 2009 Capsule motion in flow: deformation and membrane buckling. *C. R. Phys.* **10**, 764–774.

Barthès-Biesel, D. 2016 Motion and deformation of elastic capsules and vesicles in flow. *Annu. Rev. Fluid Mech.* **48**, 25–52.

Blackburn, H. M. & Lopez, J. M. 2003 The onset of three-dimensional standing and modulated travelling waves in a periodically driven cavity flow. *J. Fluid Mech.* **497**, 289–317.

Blennerhassett, P. J. & Bassom, A. P. 2002 The linear stability of flat Stokes layers. *J. Fluid Mech.* **464**, 393–410.

Blennerhassett, P. J. & Bassom, A. P. 2007 The linear stability of high-frequency oscillatory flow in a torsionally oscillating cylinder. *J. Fluid Mech.* **576**, 491–505.

Bryngelson, S. H. & Freund, J. B. 2016 Capsule-train stability. *Phys. Rev. Fluids* **1**, 033201.

Bryngelson, S. H. & Freund, J. B. 2018 Global stability of flowing red blood cell trains. *Phys. Rev. Fluids* **3**, 073101.

CAZEMIER, W., VERSTAPPEN, R. W. C. P. & VELDMAN, A. E. P. 1998 Proper orthogonal decomposition and low-dimensional models for driven cavity flows. *Phys. Fluids* **10** (7), 1685–1699.

CHANG, T. M. 2010 Blood replacement with nanobiotechnologically engineered hemoglobin and hemoglobin nanocapsules. *Wiley Intersci. Rev. Nanomed. Nanobiotechnol.* **2**, 418–430.

CORDASCO, D. & BAGCHI, P. 2013 Orbital drift of capsules and red blood cells in shear flow. *Phys. Fluids* **25**, 091902.

DAVIES, C., THOMAS, C., BASSOM, A. P. & BLENNERHASSETT, P. J. 2015 The linear impulse response of disturbances in an oscillatory Stokes layer. *Procedia IUTAM* **14**, 381–384.

DEY, N. S., MAJUMDAR, S. & RAO, M. E. B. 2008 Multiparticulate drug delivery systems for controlled release. *Trop. J. Pharm. Res.* **7** (3), 1067–1075.

DUPIRE, J., ABKARIAN, M. & VIALLAT, A. 2010 Chaotic dynamics of red blood cells in a sinusoidal flow. *Phys. Rev. Lett.* **104**, 168101.

DUPONT, C., DELAHAYE, F., BARTHÈS-BIESEL, D. & SALSAC, A.-V. 2016 Stable equilibrium configurations of an oblate capsule in simple shear flow. *J. Fluid Mech.* **791**, 738–757.

DUPONT, C., SALSAC, A.-V. & BARTHÈS-BIESEL, D. 2013 Off-plane motion of a prolate capsule in shear flow. *J. Fluid Mech.* **721**, 180–198.

EINARSSON, J., ANGILELLA, J. R. & MEHLIG, B. 2014 Orientational dynamics of weakly inertial axisymmetric particles in steady viscous flow. *Physica* D **278–279**, 79–85.

FOESSEL, E., WALTER, J., SALSAC, A.-V. & BARTHÈS-BIESEL, D. 2011 Influence of internal viscosity on the large deformation and buckling of a spherical capsule in simple shear flow. *J. Fluid Mech.* **672**, 477–486.

FREUND, J. B. & ZHAO, H. 2010 *Hydrodynamics of Capsules and Biological Cells*, chap. A. Fast high-resolution boundary integral method for multiple interacting blood cells, pp. 71–111. Chapman and Hall/CRC.

FURLOW, B. 2009 Contrast-enhanced ultrasound. *Radiol. Technol.* **80**, 547–561.

GÅSERØD, O., SANNES, A. & SKJÅK-BRÆK, G. 1999 Microcapsules of alginate–chitosan. II. A study of capsule stability and permeability. *Biomaterials* **20** (8), 773–783.

GIBBS, B. F., KERMASHA, S., ALLI, I. & MULLIGAN, C. N. 1999 Encapsulation in the food industry: a review. *Intl J. Food Sci. Neut.* **50**, 213–224.

GIORIA, R. S., JABARDO, P. J. S., CARMO, B. S. & MENEGHINI, J. R. 2009 Floquet stability analysis of the flow around an oscillating cylinder. *J. Fluids Struct.* **25**, 676–686.

GOOSEN, M. F., O'SHEA, G. M., GHARAPETIAN, H. M., CHOU, S. & SUN, A. M. 1985 Optimization of microencapsulation parameters: semipermeable microcapsules as a bioartifical pancreas. *Biotechnol. Bioengng* **27** (2), 146–150.

GUCKENBERGER, A. & GEKLE, S. 2017 Theory and algorithms to compute Helfrich bending forces: a review. *J. Phys.: Condens. Matter* **29** (20), 203001.

JUNIPER, M. 2011 Triggering in the horizontal Rijke tube: non-normality, transient growth and bypass transition. *J. Fluid Mech.* **667**, 272–308.

KIM, S. & KARRILA, S. J. 1991 *Microhydrodynamics: Principles and Selected Applications*. Butterworth-Heinemann.

KUHTREIBER, W. M., LANZA, R. P. & CHICK, W. L. 1998 *Cell Encapsulation Technology and Therapeutics*. Birkhäuser.

LAC, E., BARTHÈS-BIESEL, D., PELEKASIS, N. A. & TSAMOPOULOS, J. 2004 Spherical capsules in three-dimensional unbounded Stokes flows: effect of the membrane constitutive law and onset of buckling. *J. Fluid Mech.* **516**, 303–334.

LEELAJARIYAKUL, S., NOGUCHI, H. & KIATKAMJORNWONG, S. 2008 Surface-modified and micro-encapsulated pigmented inks for ink jet printing on textile fabrics. *Prog. Org. Coat.* **62** (2), 145–161.

LIM, F. 1984 *Biomedical Applications of Microencapsulations*, 1st edn. CRC.

LIU, J. 2003 *A First Course in the Qualitative Theory of Differential Equations*. Prentice Hall.

MARTINS, I. M., BARREIRO, M. F., COELHO, M. & RODRIGUES, A. E. 2014 Microencapsulation of essential oils with biodegradable polymeric carriers for cosmetic applications. *Chem. Engng J.* **245**, 191–200.

MIYAZAWA, K., YAJIMA, I., KANEDA, I. & YANAKI, T. 2000 Preparation of a new soft capsule for cosmetics. *J. Cosmet. Sci.* **51** (4), 239–252.

PARET, N., TRACHSEL, A., BERTHIER, D. L. & HERRMANN, A. 2015 Controlled release of encapsulated bioactive volatiles by rupture of the capsule wall through the light-induced generation of a gas. *Chem. Intl Ed.* **54** (7), 2275–2279.

PIER, B. & SCHMID, P. J. 2017 Linear and nonlinear dynamics of pulsatile channel flow. *J. Fluid Mech.* **815**, 435–480.

POP, F. 2011 Chemical stabilization of oils rich in long-chain polyunsaturated fatty acids during storage. *Food Sci. Technol. Intl* **17** (2), 111–117.

POZRIKIDIS, C. 1992 *Boundary Integral and Singularity Methods for Linearized Viscous Flow*. Cambridge University Press.

PUMHÖSSEL, T., HEHENBERGER, P. & ZEMAN, K. 2014 Reduced-order modelling of self-excited, time-periodic systems using the method of proper orthogonal decomposition and the Floquet theory. *Math. Comput. Model. Dyn. Syst.* **20** (6), 528–545.

RALLISON, J. M. & ACRIVOS, A. 1978 A numerical study of the deformation and burst of a viscous drop in an extensional flow. *J. Fluid Mech.* **89**, 191–200.

ROCHAL, S. B., LORMAN, V. L. & MENNESSIER, G. 2005 Viscoelastic dynamics of spherical composite vesicles. *Phys. Rev.* E **71**, 021905.

ROWLEY, C. W., MEZIC, I., BAGHERI, S., SCHLATTER, P. & HENNINGSON, D. S. 2009 Spectral analysis of nonlinear flows. *J. Fluid Mech.* **641**, 115–127.

SACKER, R. 1964 On invariant surfaces and bifurcation of periodic solutions of ordinary differential equations. *Tech. Rep.* IMM-NYU 333. New York University.

SCHMID, P. J. 2010 Dynamic mode decomposition of numerical and experimental data. *J. Fluid Mech.* **656**, 5–28.

SCHMID, P. J. & HENNINGSON, D. S. 2012 *Stability and Transition in Shear Flows*. Springer Science and Business Media.

SCHMID, P. J. & KYTOMAA, H. K. 1994 Transient and asymptotic stability of granular flow. *J. Fluid Mech.* **264**, 255–275.

SHEARD, G. J., FITZGERALD, M. J. & RYAN, K. 2009 Cylinders with square cross-section: wake instabilities with incidence angle variation. *J. Fluid Mech.* **630**, 43–69.

SHEARD, G. J., THOMPSON, M. C. & HOURIGAN, K. 2003 From spheres to circular cylinders: the stability and flow structures of bluff ring wakes. *J. Fluid Mech.* **492**, 147–180.

SHEARD, G. J., THOMPSON, M. C. & HOURIGAN, K. 2004 From spheres to circular cylinders: non-axisymmetric transitions in the flow past rings. *J. Fluid Mech.* **506**, 45–78.

SKALAK, R., TOZEREN, A., ZARDA, P. R. & CHIEN, S. 1973 Strain energy function of red blood cell membranes. *Biophys. J.* **13**, 245–264.

SKOTHEIM, J. M. & SECOMB, T. W. 2007 Red blood cells and other nonspherical capsules in shear flow: oscillatory dynamics and the tank-treading-to-tumbling transition. *Phys. Rev. Lett.* **98** (7), 078301.

THOMAS, C., BASSOM, A. P. & BLENNERHASSETT, P. J. 2012 The linear stability of oscillating pipe flow. *Phys. Fluids* **24**, 014106.

THOMAS, C., BLENNERHASSETT, P. J., BASSOM, A. P. & DAVIES, C. 2015 The linear stability of a Stokes layer subjected to high-frequency perturbations. *J. Fluid Mech.* **764**, 193–218.

VERHULST, F. 2006 *Nonlinear Differential Equations and Dynamical Systems*. Springer.

VERICELLA, J. J., BAKER, S. E., STOLAROFF, J. K., DUOSS, E. B., HARDIN, J. O. IV, LEWICKI, J., GLOGOWSKI, E., FLOYD, W. C., VALDEZ, C. A., SMITH, W. L., SATCHER, J. H. JR., BOURCIER, W. L., SPADACCINI, C. M., LEWIS, J. A. & AINES, R. D. 2015 Encapsulated liquid sorbents for carbon dioxide capture. *Nature Commun.* **6**, 6124.

VON KERCZEK, C. H. 1982 The instability of oscillatory plane Poiseuille flow. *J. Fluid Mech.* **116**, 91–114.

WALTER, A., REHAGE, H. & LEONHARD, H. 2001 Shear induced deformation of microcapsules: shape oscillations and membrane folding. *Colloid Surf.* **183–185**, 123–132.

WANG, Z., SUI, Y., SPELT, P. D. M. & WANG, W. 2013 Three-dimensional dynamics of oblate and prolate capsules in shear flow. *Phys. Rev.* E **88**, 053021.

ZHAO, H., ISFAHANI, A. H. G., OLSON, L. & FREUND, J. B. 2010 A spectral boundary integral method for micro-circulatory cellular flows. *J. Comput. Phys.* **229**, 3726–3744.

ZHAO, H. & SHAQFEH, E. S. G. 2013 The shape stability of a lipid vesicle in a uniaxial extensional flow. *J. Fluid Mech.* **719**, 345–361.